estimate are available in near real-time and hence the time series has been extended from May 2012 (reported last year) to October 2013 (Fig. 3.23). Furthermore, near 16°N, the MOC is being estimated by a mooring array of inverted echo sounders, current meters, and dynamic height moorings that measure the deep circulation that is the southward flowing part of the MOC conveyor belt that sends North Atlantic Deep Water towards the equator (see Send et al. 2011 for further details). For this report, the 16°N data has been updated from June 2011 to October 2013, the date of the last cruise. The updated data from all three latitudes were 90-day low-pass filtered and plotted in Fig. 3.23. The mean MOC based on these estimates decreases to the north (22.8 Sv at 16°N; 17.3 Sv at 26°N; 13.8 Sv at 41°N). Similarly, the variability decreases to the north (as described by the standard deviation: 4.2 Sv at 16°N; 3.4 Sv at 26°N; 2.9 Sv at 41°N). All three time series have a seasonal cycle, which is most prominent at 26°N and 41°N (Fig. 3.23). There are different phases for each, with 41°N having a maximum MOC in May–July, 26°N having a broad maximum in July–November (Kanzow et al. 2010), and 16°N having a maximum southward flow (and hence stronger MOC) in November–January. Of note

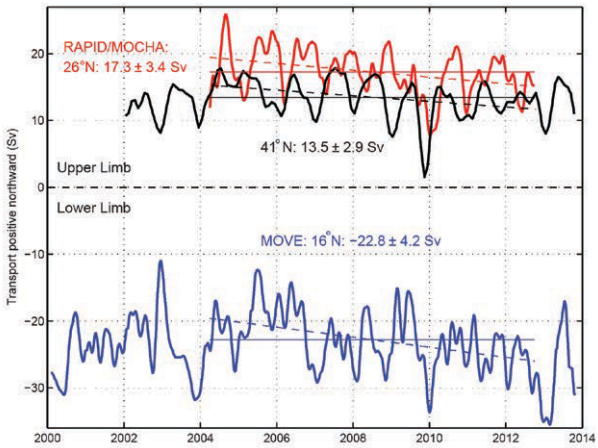

Fig. 3.23. Estimates of the MOC (Sv) in the Atlantic Ocean from the Argo/Altimetry estimate at 41°N (black; Willis 2010), the RAPID-WATCH/MOCHA/WBTS 26°N array (red; Rayner et al. 2010), and the German/NOAA MOVE array at 16°N (blue; Send et al. 2011). All time series have a three-month second-order butterworth low pass filter applied. Horizontal lines are the mean transport during similar time periods as listed in the corresponding text. Dashed lines are the trends for each series over the same time period. For the MOVE data the net zonal and vertical integral of the deep circulation represents the lower limb of the MOC (with a negative sign for the southward flow) and hence a stronger negative southward flow represents an increase in the MOC.

with the most recent data, the 16°N data has stronger southward flow, reaching filtered values above −34 Sv; the new 26°N data is slightly lower than the long-term average and the newest 41°N data is similar to the long-term average. Various authors have reported longer-term MOC trends ranging from zero (Willis 2010 using the first seven years of data from 41°N) to a −3 Sv decade^{-1} decrease (Send et al. 2011 using the first 9.5 years of data from 16°N), to the largest decrease of −5.4 Sv decade^{-1} (Smeed et al. 2014 using the first 8.5 years of data from 26°N). Using the overlapping time period of these observations (2 April 2004 to 2 October 2012) which includes more recent data than reported by Willis (2010) and Send et al. (2011), there is an insignificant trend in the MOC of −3.3 ±6.5 Sv decade^{-1} at 41°N, while at 26°N there is a strong decrease in the MOC of −5.1 ±4.1 Sv decade^{-1} (using 95% confidence limits; Fig. 3.23). However, at 16°N the deep southward flow has recently been increasing, suggesting a possible increase of the MOC at 8.4 ±5.6 Sv decade^{-1}. At 26°N where both the upper and deep southward flows are measured, the decreasing MOC is seen to be compensated by a reduction in the southward export of lower North Atlantic Deep Water (LNADW) in the depth range of 3–5 km (perhaps surprisingly there is no trend in export of upper North Atlantic Deep Water in the depth range 1.1–3 km). The decrease in export of LNADW is 4.6 ±3.9 Sv decade^{-1} (Fig. 3.22b; Smeed et al. 2014). From the full time series from 41°N and 16°N, the MOC trends decrease, becoming insignificant (−0.9 ±4.6 Sv decade^{-1} at 41°N and −2.3 ±2.9 Sv decade^{-1} at 16°N). At these time scales, there appears to be no consistent trend in the MOC at these latitudes. Note that statistically significant changes can be found using various subsets of these time series; however, the interpretation of any trend should consider regional, interannual, and decadal variability that may not be linked to longer-term trends.

i. Meridional oceanic heat transport in the Atlantic Ocean—M. O. Baringer, W. E. Johns, S. Garzoli, S. Dong, D. Volkov, and W. R. Hobbs

The meridional overturning circulation is related to the meridional heat transport (MHT) in the oceans, and the variability of MHT can impact heat storage, sea-level rise, and air-sea fluxes, and hence influence local climate on land. Time series of the oceanic heat transport are more rare than time series of the meridional overturning circulation because they involve the product of temperature and velocity to be resolved across a trans-basin section where

total mass transport can be accounted for. This report includes MHT time series data from 26°N, 41°N, and 35°S in the Atlantic Ocean.

The MHT at 26°N is based on the MOC array of moorings, cabled observations, and Argo profiling float data described in Johns et al. (2011); like the meridional overturning circulation estimates from this array (section 5h), the MHT reported this year has been updated to include new estimates from April 2011 through October 2012. At 26°N the median MHT from April 2004 to October 2012 was 1.25 ±0.36 PW (1 PW = 10^{15} W; Fig. 3.24). The MHT time series follows the general variability of the MOC time series at this latitude. The total MHT is composed of the sum of temperature transports from the Florida Current (median 2.52 ±0.25 PW standard deviation), Ekman temperature transport (0.35 ±0.29 PW), and interior ocean temperature transport (−1.60 ±0.30 PW). The annual median MHT shows a decrease in the MHT in 2009 and 2010 (including negative values in December 2010 for the 10-day low pass filtered data), which then returned to average values in 2011, reported for the first time in this report (Fig. 3.24). The MHT was fairly unremarkable in 2011 and 2012 (Fig 3.24b), except in May and June 2012 when the transport was low for that time of year. For the full time series, the Ekman transport accounts for about 60% of the variance of the MHT (0.77 correlation), while the Florida Current accounts for about 30% of the variance (0.55 correlation). Unlike the MOC, the interior circulation appears to play a lesser role in the variability overall; however, it can be a dominant factor during certain time periods (e.g., McCarthy et al. 2012). The MHT shows a statistically significant decrease of −0.3 ±0.25 PW decade^{-1} (95% confidence limits) from April 2004 to October 2012 (using the full 8.5-year time series); however, this decrease is largely due to the lows in 2009 and 2010 and is likely a signal of interannual and decadal variability rather than a longer-term secular change.

At 35°S in the South Atlantic, MHT has been estimated using a combination of expendable bathythermograph (XBT) data and Argo profiling floats (Garzoli et al. 2012; Dong et al. 2009). From July 2002 to January 2014 the median of the MHT near 35°S is 0.55 ±0.16 PW (±1 standard deviation; Fig. 3.25). At 41°N the MHT was estimated by Hobbs and Willis (2012) using altimetry and Argo profiling float data. The median MHT near 41°N has not been updated since Baringer et al. (2013), and from January 2002 to September 2010 is 0.50 ±0.10 PW. There is no significant trend at 41°N or 35°S, −0.04 ±0.23 PW and +0.12 ±0.12 PW, respectively (Fig. 3.25). The eddy-permitting global ECCO2 data synthesis (Menemenlis et al. 2005) follows nearly exactly the MHT at 41°N, while its average is too low at 26°N and 35°S; however, the correlation is actually highest at 26°N (correlation = 0.8). The state estimation is least correlated with observations at 35°S and has much larger variance in general. Overall, the heat trans-

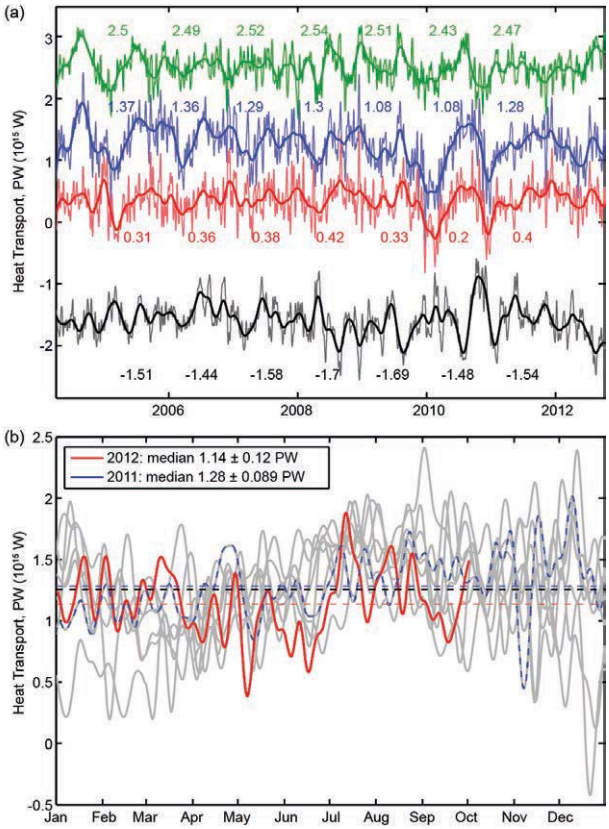

Fig. 3.24. (a) Daily estimates at 26.5°N of the strength (×10^{15} W) of the meridional heat transport (blue line) and its associated temperature transport components, the Florida Current (green), wind-driven Ekman transport (red), and the geostrophic interior (black), as measured by the UK National Environmental Research Council (NERC) Rapid Climate Change Program (RAPID-WATCH), the National Science Foundation's Meridional Overturning and Heat transport Array proposal, and the NOAA Western Boundary Time Series project (WBTS). The high frequency heat transports have a 10-day low pass filter applied to the daily values (Rayner et al. 2010), the smooth curve (heavy lines) represent 90-day low pass filtered data. The annual averages of the transports for each year are shown in the associated color text. (b) MHT (×10^{15} W) from 2012 (red), 2011 (dashed blue), and all other years (gray) plotted as a function of month. Thin horizontal dashed lines are annual mean values for 2012 (red), 2011 (blue), and all years (black).

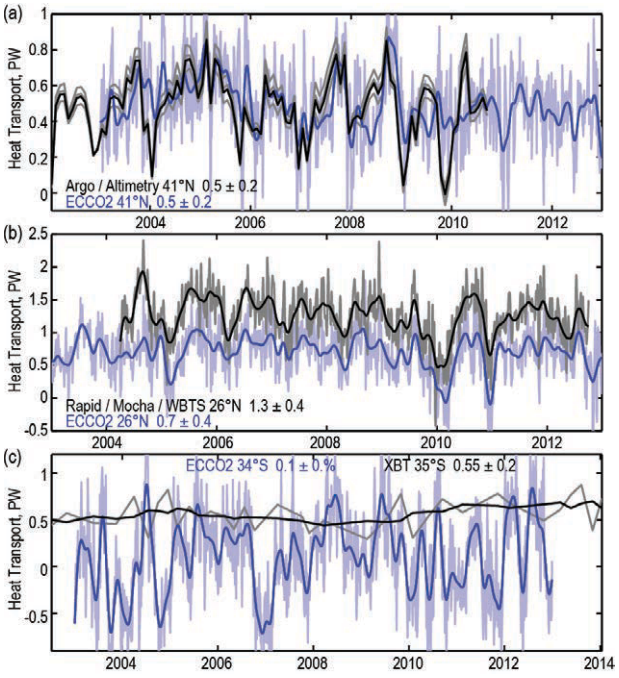

Fig. 3.25. Observed time series of meridional heat transport (PW) at (a) 41°N (profiling floats), (b) 26°N (mooring/hydrography) and (c) 30°–35°S (XBTs) in the Atlantic compared to the monthly estimates from the ECCO2 state estimation (light blue line) and a 3-month low pass of ECCO2 data (blue line). In (a) the black line is the estimate MHT and the gray lines represents the error in the estimate (Hobbs and Willis 2012). In (b) the black line is the observed data filtered with a 3-month low pass filter and the gray lines are the underlying 12-hourly data. In (c) the gray line is the quarterly estimated MHT from XBTs and the black line is a yearly boxcar filter to those quarterly estimates.

port was fairly average in 2012. In 2013, near 35°S the MHT was larger than usual (with August 2013 data falling higher than 97.5% of the other estimates at this latitude).

j. Sea level variability and change—M. A. Merrifield, P. Thompson, E. Leuliette, R. S. Nerem, B. Hamlington, D. P. Chambers, G. T. Mitchum, K. McInnes, J. J. Marra, M. Menéndez, and W. Sweet

Global mean sea level (GMSL) continued to rise during 2013, on pace with a 20-year linear trend of 3.2 mm yr^{-1} (Fig. 3.26a). A portion of this trend (0.5 mm yr^{-1}) has been attributed to natural variability associated with the Pacific decadal oscillation (PDO; Hamlington et al. 2013) as well as to ongoing contributions from the melting of glaciers and ice sheets and ocean warming (Rhein et al. 2013). While interannual variations in GMSL occur regularly, there is no evidence of a hiatus in sea-level rise as has been observed in the surface temperature record over the last decade (Trenberth and Fasullo 2013).

Interannual fluctuations in GMSL about the trend are largely linked to exchanges of water with the continents due to changes in precipitation patterns, including the pronounced minima of 2010–11 and maxima of 2012–13 (Boening et al. 2012; Fasullo et al. 2013). Over 2011–12, global mean sea level rose at ~10 mm yr^{-1} as it recovered from the 2010–11 minima. This is also reflected in the changes in global mean ocean mass measured by satellite gravimetry (Fig. 3.26a) and in global mean continental water storage (see section 2d6). The highest regional sea surface height (SSH) trends occur in the western equatorial Pacific with strong positive trends extending across northern Australia (White et al. 2014, manuscript submitted to *Earth-Sci. Rev.*) and associated weak to negative trends along the eastern boundary of the Pacific (Fig. 3.26b). The regional sea level trend pattern is reflected in the Southern Oscillation and Pacific decadal oscillation indices in the Pacific (Merrifield et al. 2012; Zhang and Church 2012) and northern Australia (White et al. 2014, manuscript submitted to *Earth-Sci. Rev.*) and is a result of multidecadal

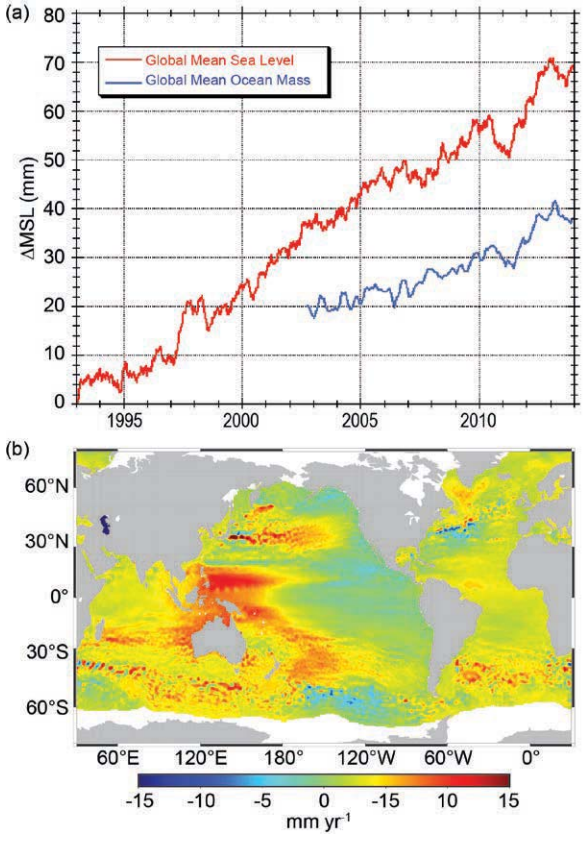

Fig. 3.26. (a) Global mean sea level (mm yr^{-1}) and global mean ocean mass (ppm; seasonal variations removed, 60-day smoothing applied). (b) Regional SSH trends (mm yr^{-1}) 1993–2013.